Independently Tunable Triple Fano Resonances in Plasmonic Waveguide Structure and Its Applications for Sensing

Qiaohua Wu
Northeast Forestry University
Yingqiu Zhang
Northeast Forestry University
Desheng Qu
Northeast Forestry University
Chunlei Li (licl915@163.com)
Northeast Forestry University

Research Article

Keywords: Surface plasmon polaritons, Fano resonances, Independently tunable, Sensing

Posted Date: April 14th, 2022

DOI: https://doi.org/10.21203/rs.3.rs-1536394/v1

Abstract

A surface plasmon polaritons (SPPs) waveguide structure composed of a metal-insulator-metal (MIM) waveguide with a baffle, a special square cavity (SSC) and a ring cavity (RC), is proposed to realize independent tuning of triple Fano resonances. Using the finite element method (FEM), the magnetic field distributions and optical transmission spectra of the structure are analyzed in detail. The simulation results show that the structure achieves triple Fano resonances originated from two different mechanics. One of Fano resonances occurs in the RC, and the others occur in SSC. By regulating the structural parameters of the SSC and RC, respectively, these Fano resonances can be well tuned independently, which provides flexibility for the structure to be applied to optical devices. In addition, the structure exhibits great performances in refractive index sensing and bio-sensing. The maximum sensitivity of refractive index sensing achieves 2350 nm/RIU, and there is a good linear relationship between resonance wavelength and refractive index. Due to great sensitivity and independent tunability, the SPPs waveguide structure may be potentially used in micro-nano optical devices, especially in optical on-chip sensor.

Introduction

Surface plasmon polaritons (SPPs) are evanescent waves that propagate along a metal-insulator interface. Those can break through the optical diffraction limit and confine the energy in deep-subwavelength dimensions [1–4], rendering them prospective for application in miniaturized optical devices. In recent years, a large number of optical devices based on SPPs have been proposed [5–8]. Among them, the SPPs waveguide structure based on Fano resonance has attracted extensive attention of researchers owning to the sharp asymmetric transmission peak [9–11]. In the SPPs waveguide structure, Fano resonance is formed by coupling of local discrete states and broad continuous states [12, 13]. Unlike Lorentz resonance, the transmission spectrum of Fano resonance shows sharp and asymmetric transmission peaks [14–16]. Meanwhile, the SPPs waveguide structure based on Fano resonance is sensitive to the refractive index of insulator. Thus, it's widely used in the field of micro-nano optical sensing [17–19].

Compared with single Fano resonance, multiple Fano resonances are more beneficial in bio-chemical sensing, refractive index sensing and concentration detection [7, 20–22]. Multiple Fano resonances are becoming more and more important and intense efforts have been devoted to achieve multiple Fano resonances [23–26]. Liu et al. [7] proposed a refractive index sensing structure based on double Fano resonance and discussed its application in hemoglobin concentration detection. Xu et al. [21] reported a nanosensor with high refractive index sensitivity based on double Fano resonances. The application in temperature sensing and glucose concentration detection was exhibited. Fang et al. [27] realized multiple Fano resonances in an end-coupled metal-insulator-metal (MIM) waveguide system which gained high figure of merit (FOM) and high sensitivity. However, owing to the multiple Fano resonances are usually triggered by the collective behavior of the whole SPPs systems, it is hard to achieve independent

tunability for multiple Fano resonances. The research should be paid more attention to increase the flexibility of device fabrications and the manipulation of optical transmission.

In this paper, independently tunable triple Fano resonances are realized in designed SPPs waveguide structure which is composed of two independent resonators (special square cavity (SSC) and ring cavity (RC)) coupled with a defective MIM waveguide. The Fano resonances can be tuned independently by adjusting the structural parameters of the SSC and RC respectively. Its application as a refractive index sensor is disscussed and the highest refractive index sensitivity is up to 2350 nm/RIU. Based on the refractive index sensing, the structure can also be used for glucose concentration detection and the maximal sensitivity of glucose concentration detection is 0.266 nm/(g/L). Benefited from the independent tuning ability of multiple Fano resonances and high refractive index sensitivity, the structure has significant potential applications in the field of integrated micro-nano optical sensing.

Structure And Theory

Figure 1 shows a schematic diagram of designed MIM waveguide structure which consists of a bus waveguide with baffle, SSC and RC. The white and gray parts denote silver and insulator, respectively. The SSC consists of a circle with radius R and a square with side length $2R+2d$, d represents minimum width in the SSC. The inner and outer radii of the RC are r_1 and r_2, respective. Therefore, the effective radius of the RC can be defined as $r=(r_1+r_2)/2$. The thickness of the baffle is fixed at $t=10$ nm. The width of bus waveguides and RC are fixed at $w=50$ nm to ensure that only one fundamental transverse magnetic (TM_0) can exist and propagate [28].

For TM_0 mode, the dispersion relationship of SPPs in MIM waveguide can be expressed as the following formula [29]:

$$\varepsilon_{\mathrm{i}}\sqrt{\beta^2-\varepsilon_{\mathrm{m}}{k_0}^2}+\varepsilon_{\mathrm{m}}\sqrt{\beta^2-\varepsilon_{\mathrm{i}}{k_0}^2}\tanh\left(\frac{\sqrt{\beta^2-\varepsilon_{\mathrm{i}}{k_0}^2}}{2}w\right)=0,$$

1

where β represents the propagation constant of SPPs, k_0 represents the wave vector in vacuum, ε_m and ε_i represent the relative dielectric constant of silver and insulator, respectively. The value of ε_m can be calculated by Drude model [20]:

$$\varepsilon_m(\omega)=\varepsilon_\infty-\frac{{\omega_p}^2}{\omega(\omega+i\gamma)}$$

2

,

Where, $\varepsilon_\infty = 3.7$ is the relative dielectric constant at infinity, $\omega_p = 9.1\ \mathrm{eV}$ is the plasma frequency, $\gamma = 0.018\ \mathrm{eV}$ represents the loss of metallic silver, and ω represents angular frequency of incident wave.

When the incident SPPs propagates along the *x* axis in the waveguide, parts of them can couple into the resonant cavity and generate phase change. When the phase-match condition is satisfied, resonance phenomenon will appear. The resonance wavelength (λ_{res}) can be described by [30, 31]:

$$\lambda_{\mathrm{res}} = \frac{L_{\mathrm{eff}} n_{\mathrm{eff}}}{m},$$

3

where $L_{\mathrm{eff}}$is the effective length of the resonant cavity, *m* is resonance mode order, and n_{eff}represents the real part of effective refractive index and can be derived by [22]:

$$n_{\mathrm{eff}} = \mathrm{Re}\left(\beta / k_0\right).$$

4

The propagation properties of the SPPs are analyzed by the finite element method (FEM). The perfect matching layers (PMLs) are set at each boundary of the simulation area to absorb the escaping electromagnetic waves. The fine triangular meshes are selected to ensure the convergence and accuracy of the simulation results, and the maximum triangular mesh size is 10 nm.

Results And Discussion

Formation mechanism of Fano peaks

In order to investigate the optical properties of the structure, the transmission spectra of the structure without baffle, the MIM waveguide with baffle, and the whole structure are shown in Fig. 2. The geometric parameters of the structure are set as *r* = 180 nm, *R* = 180 nm, *d* = 20 nm, and *g* = 10 nm. For the structure without baffle, as shown in the red line, there are three transmission dips at 1390 nm, 1800 nm, and 2235 nm in the transmission spectrum, which can be treated as narrow discrete states. Meanwhile, the MIM waveguide with baffle can formed a broad continuum state as shown in the black line. For the whole structure, as a result of the interference of the discrete states and the continuum state, there are three Fano peaks (FR1, FR2, and FR3) at the wavelengths of 1364 nm, 1790 nm, and 2222 nm, as shown in the green line.

To further understand the mechanism of Fano resonances of the designed structure, the magnetic field distributions (Hz) at the resonant wavelengths are simulated as shown in Fig. 3. It can be seen that the energy is almost distributed in the SSC at the wavelengths of 1364 nm and 2222 nm. On the contrary,

most of the energy is distributed in the RC at the wavelength of 1790 nm. This phenomenon indicates that both FR1 and FR3 may be more effected by SSC and the RC may have more powerful affect on FR2. The two magnetic field distributions of FR1 and FR3 show that the SPPs coupled into SSC meet the resonance conditions, and the resonance mode orders at FR1 and FR3 are 2 and 1, respectively. The Fig. 3(b) shows that the SPPs in RC produce a phase shift of 2π and the resonance mode order is 1.

Tunable Fano resonance and its applications for sensing

First, we investigate the influences of the SSC and RC sizes on Fano resonances of the structure. In Fig. 4(a), the inner radius *R* of SSC increases from 180 nm to 200 nm in step of 5 nm, and the structural parameter *d* is fixed at 20 nm. The approximately linear relationships between the resonance wavelengths and the inner radius of the SSC are shown in Fig. 4(b). When the structure parameter *R* increases from 180 nm to 200 nm, the wavelengths of FR1 and FR3 are increased by 100 nm and 230 nm, respectively, but FR2 keeps unchanged. Analyzing of these results, FR1 and FR3 meet the resonance conditions in SSC, while FR2 meets the resonance conditions in RC. According to Eq. (3), only changing the size of SSC will change the wavelengths of FR1 and FR3, while that of FR2 remains unchanged. Figure 5(a) shows the transmission spectra for different effective radii of the RC from 205 nm to 235 nm with step of 10 nm, and the linear fitting curves between the resonance wavelengths and the effective radius of the RC are shown in Fig. 5(b). As the effective radius *r* increases, the wavelength of FR2 increases from 1790 nm to 2048 nm, and those of FR1 and FR3 remain unchanged. This phenomenon shows that the size of RC only affects FR2. Therefore, FR1 and FR3 can be tuned by changing the structural parameter *R* of the SSC, while FR2 can be tuned by changing the effective radius of the RC. The triple Fano resonances can be well tuned independently.

Successively, we investigate the effect of the refractive index of the insulator in the resonators on the position of Fano resonance peaks. The refractive indexes of the insulator in the SSC and RC increases from 1.0 to 1.12 with a step of 0.04, and the other area refractivity remains unchanged. The corresponding transmission spectra is exhibited in Fig. 6(a). It can be seen that the resonance wavelengths of the triple Fano resonances all appear obvious red-shifts and the Fano resonances are sensitive to the insulator refractive index of the resonators. The phenomenon can be explained by Eq. (1)-(4). With the increase of the refractive index of the insulator in the SSC and RC, the effective refractive index increases, and then the resonant wavelength red shift. Figure 6 (b) shows the linear fitting relationship between the resonant wavelengths of the three Fano peaks and the refractive index of the insulator in the SSC and RC. It can be seen that FR1, FR2, and FR3 all have good performances in linearity. The linear correlation coefficients of FR1, FR2, and FR3 are 0.99992, 0.9993, and 0.99995, respectively.

Based on the linear adjustment of Fano resonance by refractive index of insulator, the designed SPPs waveguide can be used for the refractive index sensing. As an important index for evaluating sensing performance, sensitivity is defined as [32–34]$S = \Delta\lambda / \Delta n$, where Δn is the change of the refractive index of the insulator in the resonant cavities, and $\Delta\lambda$ is the variation of the corresponding resonant wavelength. Therefore, the refractive index sensitivities of FR1, FR2 and FR3 can be expressed by the

slope of the fitting lines in Fig. 6(b). Those are 1330 nm/RIU, 1785 nm/RIU and 2235 nm/RIU, respectively. It can be seen that FR3 has the largest sensitivity compared with FR1 and FR2. Based on the same dielectric properties of material for RC and SSC, FR3 has the greater sensitivity due to its higher resonant wavelength [35]. In addition, another key factor to sensing performance is FOM which is defined as [36] $\mathrm{FOM} = \Delta T / T \Delta n$. Where represents the transmittance and ΔT represents the transmittance change. The structure parameters are the same as the initial values. The FOM values at different wavelengths are shown in Fig. 7. It can be seen that the highest FOM reaches 3387 at 2395 nm. This result shows that the Fano peak is very sharp, which is conducive to the accurate measurement of the peak position [37].

Based on the refractive index sensing performance, the SPPs waveguide structure is suitable for detecting biological parameters that have definite correlation with refractive index, such as the glucose solution concentration. The refractive index of glucose solution can be expressed as [38]:

$$n_{\mathrm{glucose}} = 1.1889 \times 10^{-4} C + 1.33230545,$$

5

where n_{glucose} is the refractive index of solution, C represents the concentration of glucose solution. In Fig. 8(a), the concentration of glucose solution in the SSC and RC increases from 0 g/L to 400 g/L with a step of 100 g/L. According to Eq. (5), the refractive index of the resonators can be calculated. The simulation results show that the resonance wavelengths of the triple Fano resonances exhibit red-shifts with the increase of solution concentration. The linear fitting relationship between resonant wavelengths and solution concentration is shown in Fig. 7(b). The slope of fitting straight lines of FR1, FR2 and FR3 are 0.164, 0.214 and 0.266, respectively. The linear correlation coefficients of FR1, FR2 and FR3 are 0.99921, 0.99965, and 0.99977, respectively. Exploiting the equation $S_{\mathrm{glucose}} = \Delta \lambda / \Delta C$, the calculated sensitivity of glucose solution sensing for FR1, FR2 and FR3 are 0.164 nm/(g/L), 0.214 nm/(g/L) and 0.266 nm/(g/L), respectively. Therefore, the concentration of glucose solution in the resonant cavity can be detected according to the resonant wavelengths.

Conclusions

In summary, triple Fano resonances are realized in a proposed SPPs waveguide structure which consists of two different resonators and a MIM waveguide with baffle. By adjusting the inner radius of the SSC or the effective radius of the RC, the Fano resonances can be well tuned independently. Furthermore, the structure can be used for refractive index sensing with a great sensitivity of 2235 nm/RIU and a high FOM of 3387. Based on great sensitivity, the structure for detecting glucose concentration can realize the maximal sensitivity of 0.266 nm/(g/L). These results show the structure may be applied in high-performance optical integrated sensing devices.

Declarations

Author Contribution Methodology: Wu Qiaohua. Review and editing: Li Chunlei*, Zhang Yingqiu and Qu Desheng. Wring-original draft preparation: Wu Qiaohua. Review, editing, supervision and Funding acquisition: Li Chunlei*. All author read and approved the final manuscript to be published.

Funding This work was supported by
the Fundamental Research Funds for the Central Universities (2572021DJ05).

Data Availability The data that support the plots within this paper can be available from the corresponding author upon reasonable request.

Code Availability

Ethics Approval Not applicable

Consent to Participate Not applicable

Consent of Publication Not applicable

Conflict of Interest The author declares no competing interests

Publisher's Note Springer Nature remains neutral with regard to jurisdictional claims in published maps and institutional affiliations.

References

1. Barnes, W.L., A. Dereux, and T.W. Ebbesen (2003) Surface plasmon subwavelength optics. Nature 424(6950): 824–830
2. Yin, Y., et al. (2012) Plasmonic nano-lasers. Nano Energy 1(1): 25–41
3. Zafar, R. and M. Salim (2015) Achievement of Large Normalized Delay Bandwidth Product by Exciting Electromagnetic-Induced Transparency in Plasmonic Waveguide. IEEE J. Quantum Electron. 51(10): 7200306
4. Wang, M., et al. (2019) Fano Resonance in an Asymmetric MIM Waveguide Structure and Its Application in a Refractive Index Nanosensor. Sensors 19(4): 791
5. Qi, Y., et al. (2020) Tunable sharp resonances based on multimode interference in a MIM-ring coupling plasmonic resonator system. Epl 132(2): 27001
6. Stevenson, P.R., et al. (2020) Active Plasmonics and Active Chiral Plasmonics through Orientation-Dependent Multipolar Interactions. Acs Nano 14(9): 11518–11532
7. Liu, X., et al. (2020) Fano resonance based on D-shaped waveguide structure and its application for human hemoglobin detection. APPl. Opt. 59(21): 6424–6430
8. Li, M., et al. (2021) Two types of corner states in two-dimensional photonic topological insulators. J. Appl. Phys. 129(6): 063104

9. Xiao, G., et al. (2021) High Sensitivity Plasmonic Sensor Based on Fano Resonance with Inverted U-Shaped Resonator. Sensors 21(4): 1164
10. Wang, Y., Z.-L. Hou, and L. Yu (2021) Plasmonic nanosensor based on sharp Fano resonances induced by aperture-coupled slot system. Opt. Commun. 480: 126438
11. Shen, F., et al. (2021) Investigation on the Fano-Type Asymmetry in Atomic Semiconductor Coupled to the Plasmonic Lattice. Acs Photonics 8(12): 3583–3590
12. Chen, Z., et al. (2016) Side-Coupled Cavity-Induced Fano Resonance and Its Application in Nanosensor. Plasmonics 11(1): 307–313
13. Zhang, Y., et al. (2015) A graphene based tunable terahertz sensor with double Fano resonances. Nanoscale 7(29): 12682–12688
14. Wan, F., et al. (2016) High sensitivity optical waveguide accelerometer based on Fano resonance. APPl. Opt. 55(24): 6644–6648
15. Chen, Z., et al. (2015) Sharp Trapped Resonances by Exciting the Anti-symmetric Waveguide Mode in a Metal-Insulator-Metal Resonator. Plasmonics 10(1): 131–137
16. Cao, T., et al. (2016) Fano resonant Ge2Sb2Te5 nanoparticles realize switchable lateral optical force. Nanoscale 8(10): 5657–5666
17. Wen, K., et al. (2015) Fano Resonance with Ultra-High Figure of Merits Based on Plasmonic Metal-Insulator-Metal Waveguide. Plasmonics 10(1): 27–32
18. Zhao, T. and S. Yu (2018) Ultra-High Sensitivity Nanosensor Based on Multiple Fano Resonance in the MIM Coupled Plasmonic Resonator. Plasmonics 13(4): 1115–1120
19. Kazanskiy, N.L., S.N. Khonina, and M.A. Butt (2020) Plasmonic sensors based on Metal-insulator-metal waveguides for refractive index sensing applications: A brief review. Phys. E 117: 113798
20. Wang, J., et al. (2013) Double Fano resonances due to interplay of electric and magnetic plasmon modes in planar plasmonic structure with high sensing sensitivity. Opt. Express 21(2): 2236–2244
21. Xu, D., et al. (2021) A Nanoscale Structure Based on a Ring With Matchstick-Shape Cavity for Glucose Concentration and Temperature Detection. IEEE Sens. J. 21(4): 4442–4450
22. Zhang, X., et al. (2018) Refractive Index Sensor Based on Fano Resonances in Plasmonic Waveguide With Dual Side-Coupled Ring Resonators. Photonic Sens 8(4): 367–374
23. Le, K.Q., A. Alu, and J. Bai (2015) Multiple Fano interferences in a plasmonic metamolecule consisting of asymmetric metallic nanodimers. J. Appl. Phys. 117(2): 023118
24. Liu, S.-D., et al. (2016) Polarization-Independent Multiple Fano Resonances in Plasmonic Nonamers for Multimode-Matching Enhanced Multiband Second-Harmonic Generation. Acs Nano 10(1): 1442–1453
25. Chen, Z., et al. (2020) Double Fano resonances in hybrid disk/rod artificial plasmonic molecules based on dipole-quadrupole coupling. Nanoscale 12(17): 9776–9785
26. Shlesinger, I., et al. (2021) Integrated Molecular Optomechanics with Hybrid Dielectric-Metallic Resonators. Acs Photonics 8(12): 3506–3516

27. Fang, Y., et al. (2019) Multiple fano resonances in an end-coupled MIM waveguide system. Opt. Commun. 452: 12–17
28. Gai, H., J. Wang, and Q. Tian (2007) Modified Debye model parameters of metals applicable for broadband calculations. APPl. Opt. 46(12): 2229–2233
29. Chen, Z., et al. (2015) Tunable Electromagnetically Induced Transparency in Plasmonic System and Its Application in Nanosensor and Spectral Splitting. IEEE Photon. J. 7(6): 1
30. Hocini, A., et al. (2020) A high-sensitive sensor and band-stop filter based on intersected double ring resonators in metal-insulator-metal structure. Opt. Quantum Electron. 52(7): 336
31. Li, C., et al. (2017) Multiple Fano Resonances Based on Plasmonic Resonator System With End-Coupled Cavities for High-Performance Nanosensor. IEEE Photon. J. 9(6): 4801509
32. Rakhshani, M.R. (2021) Refractive index sensor based on dual side-coupled rectangular resonators and nanorods array for medical applications. Opt. Quantum Electron. 53(5): 232
33. Chen, Y., Y. Xu, and J. Cao (2019) Fano resonance sensing characteristics of MIM waveguide coupled Square Convex Ring Resonator with metallic baffle. Results Phys. 14: 102420
34. Chen, J., et al. (2021) Fano resonance in a MIM waveguide with double symmetric rectangular stubs and its sensing characteristics. Opt. Commun. 482: 126563
35. Miller, M.M. and A.A. Lazarides (2005) Sensitivity of metal nanoparticle surface plasmon resonance to the dielectric environment. J. Phys. Chem. B 109(46): 21556–21565
36. Yu, S., et al. (2019) Tuning Multiple Fano Resonances for On-Chip Sensors in a Plasmonic System. Sensors 19(7): 1559
37. Otte, M.A., et al. (2010) Identification of the Optimal Spectral Region for Plasmonic and Nanoplasmonic Sensing. Acs Nano 4(1): 349–357
38. Liu, X., et al. (2021) Independently tunable triple Fano resonances based on MIM waveguide structure with a semi-ring cavity and its sensing characteristics. Opt. Express 29(13): 20829–20838

Figures

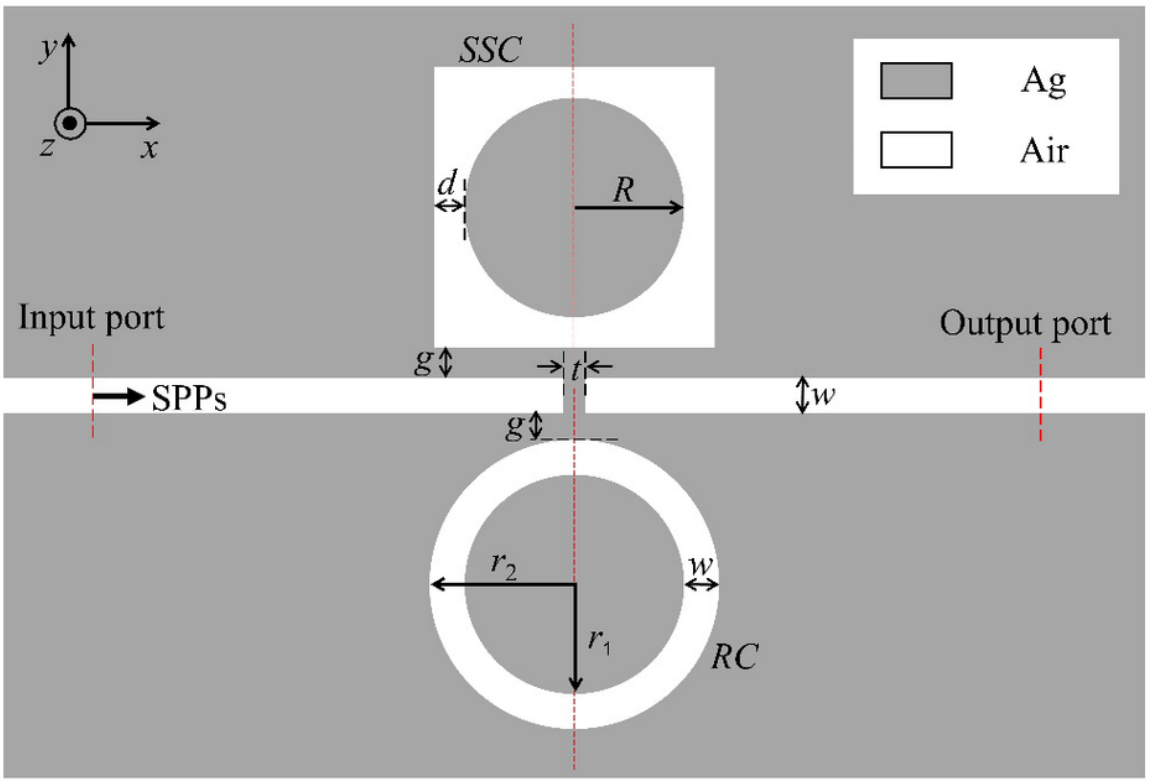

Figure 1

Schematic diagram of SPPs waveguide structure

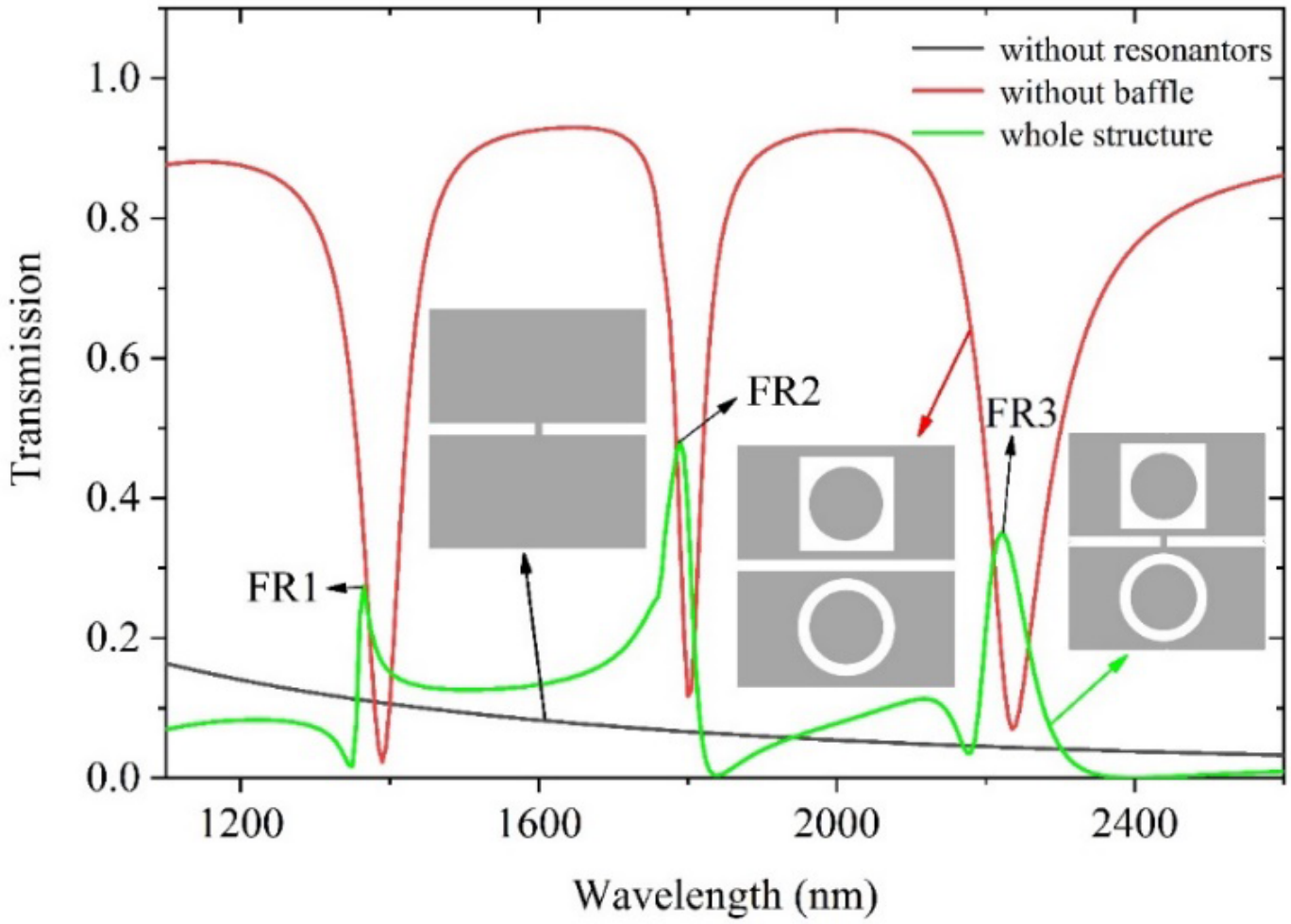

Figure 2

Transmission spectra of the structure without baffle (red line), the MIM waveguide with baffle (black line), and the whole structure (green line).

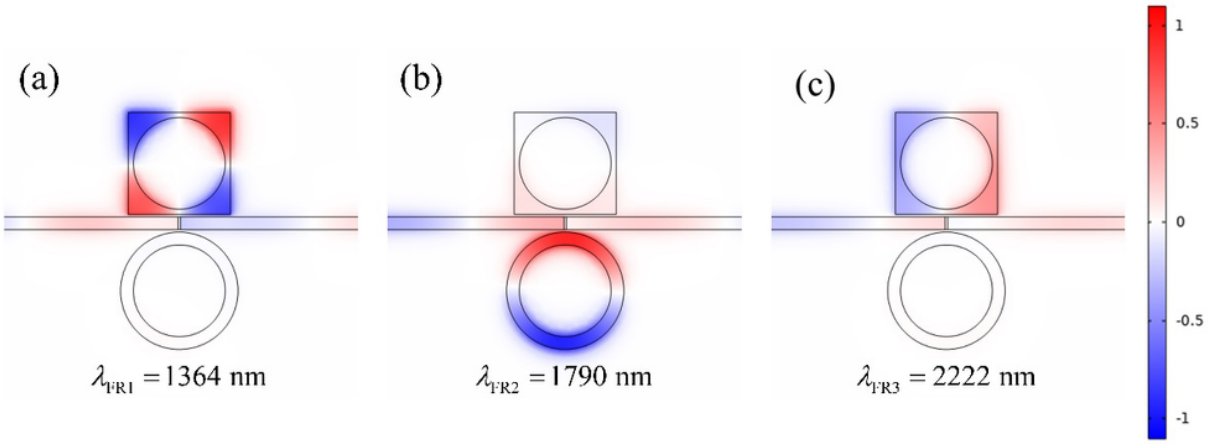

Figure 3

Magnetic field distributions at the wavelengths of Fano peaks

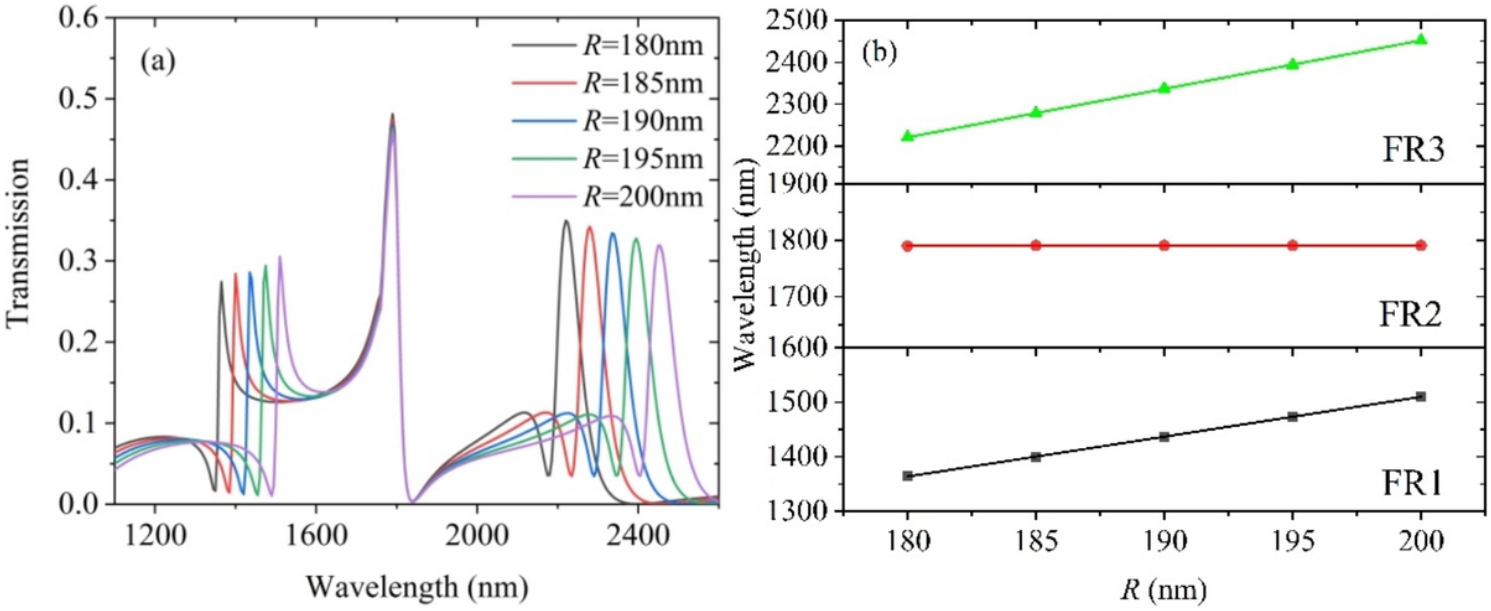

Figure 4

(a) Transmission spectra of the structure in various inner radius of the SSC (*r*=205 nm, *d*=20 nm, *g*=*t*=10 nm, and *w*=50 nm). (b) Relationships between the resonance wavelengths and the inner radius of the SSC.

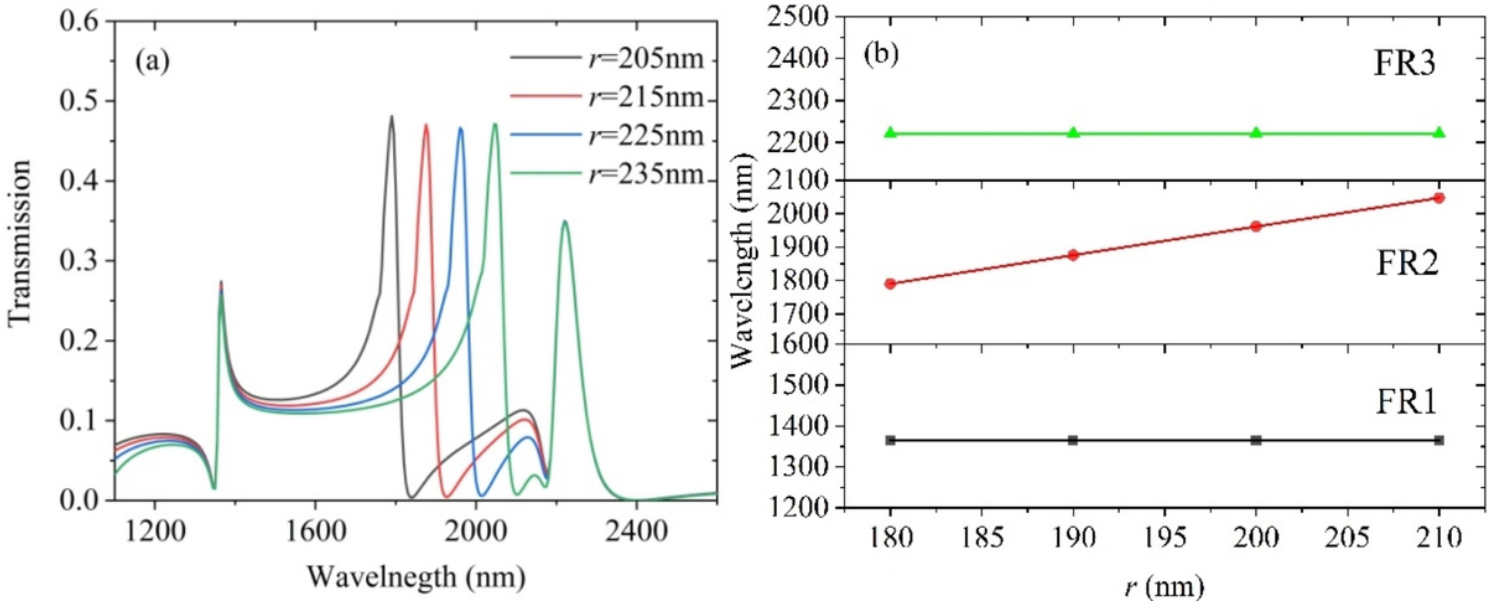

Figure 5

(a) Transmission spectra of the structure in various effective radius *r* of the RC (*R*=180 nm, *d*=20 nm, *g*=*t*=10 nm, and *w*=50 nm). (b) Relationships between the resonance wavelengths and the effective radius of the SSC.

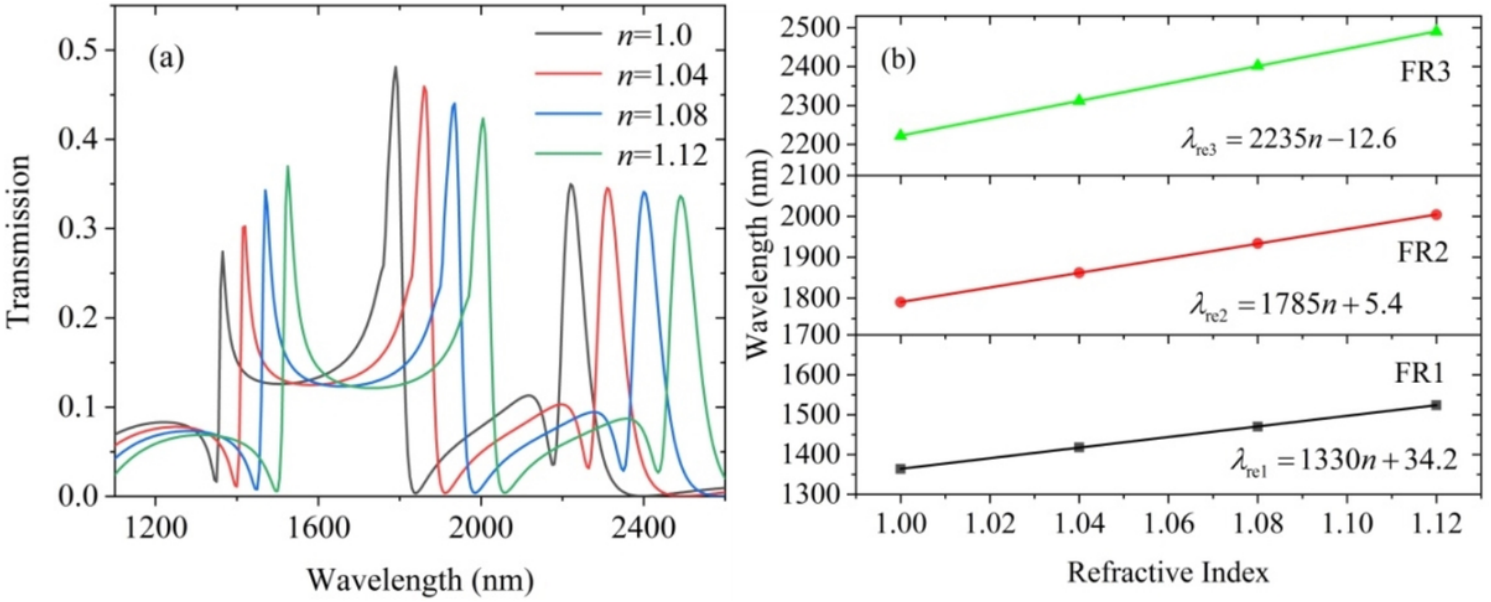

Figure 6

(a) Transmission spectra of the structure at various refractive index of insulator in the SSC and RC. (b) Linear fitting between the resonant wavelengths and the refractive index of insulator in the SSC and RC.

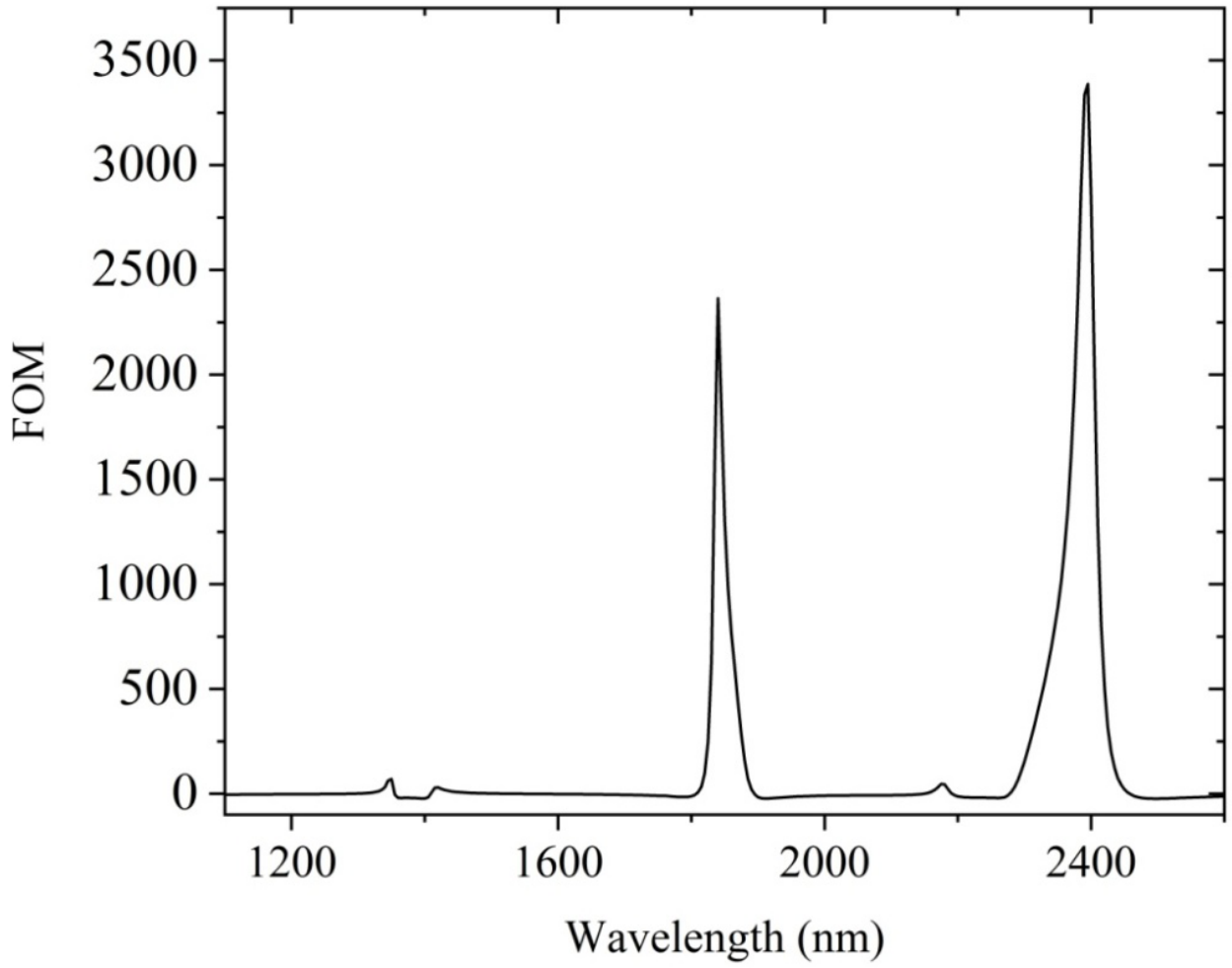

Figure 7

The FOM of designed structure at different wavelengths

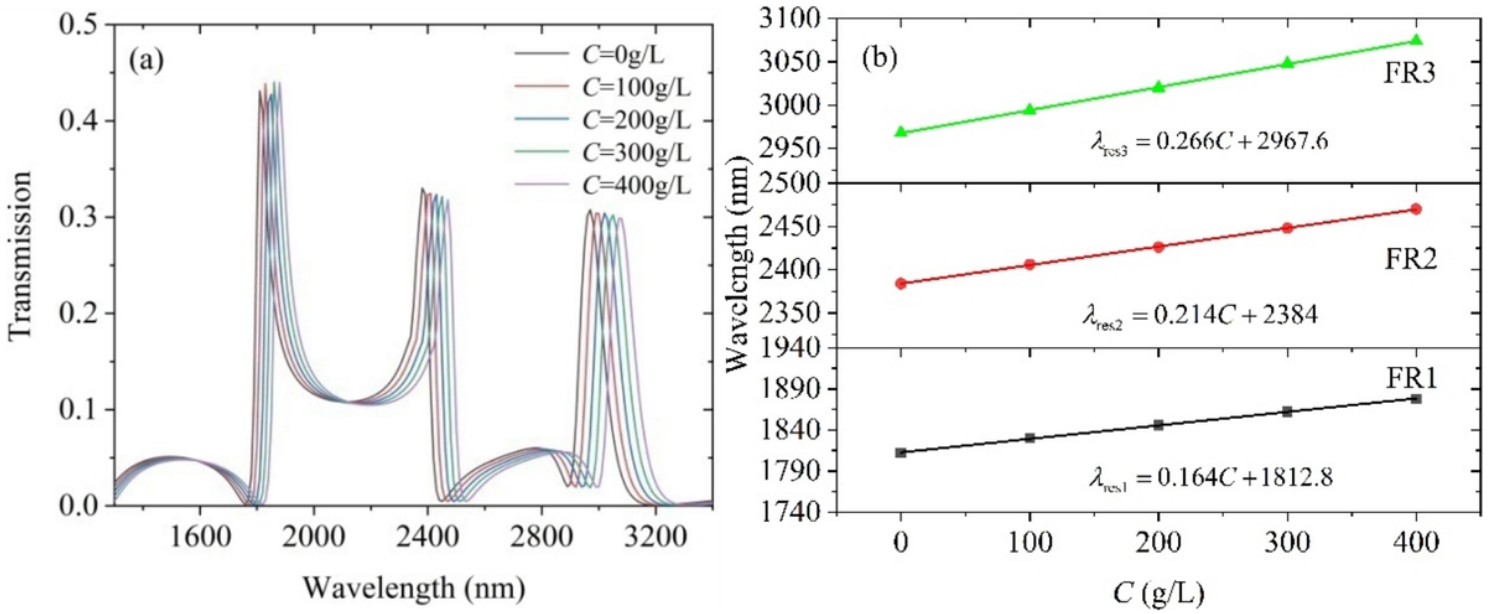

Figure 8

(a) Transmission spectra at different concentrations of glucose solution. (b) Linear fitting between resonant wavelength and solution concentration